Band Structure of HgSe: Band Parameter Determinations from Effective-Mass Data, and Concentration Dependence and Anisotropy of Beating Effects in the Shubnikov–de Haas Oscillations*

D. G. Seiler
Department of Physics, North Texas State University, Denton, Texas 76203
and
R. R. Galazka† and W. M. Becker
Department of Physics, Purdue University, Lafayette, Indiana 47907
(Received 14 August 1970; revised manuscript received 8 February 1971)

We use an E-vs-k relation (derived by Kane from the $\vec{k}\cdot\vec{p}$ method) which includes a finite spin-orbit splitting Δ and the effects of the higher band interactions to calculate the concentration dependence of the effective mass of electrons in the Γ_8 conduction band of HgSe. The calculation employs numerical methods derived earlier by us for the analyses of Shubnikov–de Haas data relating to warping effects in the same band. We find a good fit to the observed concentration dependence of the effective mass reported by Whitsett from Shubnikov–de Haas results, using the following values of the band parameters: $P=7.2\times10^{-8}$ eV cm, $E_g=-0.22$ eV, $\Delta=0.45$ eV and $A'=0$, $B'=0$, $M=-5$, $L'=-2$, and $L-M-N=4$ in units of $\hbar^2/2m_0$. The close agreement between the theory and experiment indicates that a finite Δ and the inclusion of higher-band interactions should be considered in the evaluation of band parameters from experimental results in HgSe. Beating patterns in the Shubnikov–de Haas oscillations in n-HgSe were initially reported by Whitsett. In this paper, we present the results of an experimental investigation which examines in detail the dependence of the beating patterns on electron concentration and magnetic field direction. The concentration range studied extended from 4.69×10^{17} to 3.73×10^{18} cm^{-3}. Magnetic field strengths up to 80 kOe were employed in the measurements. The results are similar to the earlier observations of Whitsett; namely, two nodes or minima in the oscillatory amplitude occur for $\vec{B}\parallel\langle111\rangle$, one minimum for $\vec{B}\parallel\langle100\rangle$, and no minima for $\vec{B}\parallel\langle110\rangle$. For the orientations $\vec{B}\parallel\langle111\rangle$ and $\vec{B}\parallel\langle100\rangle$, the Landau-level numbers of the nodal positions are found to be independent of concentration. The variations of the nodal positions with magnetic field direction have been examined for the orientations $\vec{B}\perp\vec{I}\parallel\langle110\rangle$ and $\vec{B}\perp\vec{I}\parallel\langle100\rangle$. Comparison of the results with published data on the III-V semiconductor GaSb indicates that the orientational effects may be a general feature of the beating in zinc-blende structures. The results are analyzed in terms of a semiclassical model of two Fermi surfaces split by inversion asymmetry, using the band parameters derived from the effective-mass analysis. This model predicts the observed concentration dependence of the beating frequency for $\vec{B}\parallel\langle111\rangle$, assuming that the two nodal points seen for this orientation are related by simple beating. The calculated splitting of the surfaces, derived from this model, is compared with the predictions of Roth's nonclassical model which involves interaction between electron spin and external magnetic fields.

I. INTRODUCTION

In an earlier paper, Galazka, Seiler, and Becker[1] (GSB) reported the results of an experimental investigation of the Shubnikov–de Haas (SdH) effect in n-HgSe. From the analysis presented, it was concluded by the authors that the conduction band in HgSe has Γ_8 symmetry, and a value for the warping parameter was determined. Whitsett[2] had previously reported effective-mass determinations in n-HgSe from SdH measurements. Both he and other authors have interpreted effective-mass results on the basis of somewhat more restrictive band models than were considered by GSB. In the first part of the present work, we undertake an analysis of Whitsett's results based on the band model used by GSB. Next, we give new experimental measurements on beating effects in the SdH oscillations in HgSe; these data are presented together with an extension of the GSB analysis to include the influence of inversion asymmetry. In the GSB paper, analytic expressions relating the SdH frequency anisotropy to warping of the $k=0$ conduction band are listed only in summary form. Since these same expressions are also employed in the present paper, we outline their derivation in an Appendix, and give the extension necessary to include inversion-asymmetry splitting.

A. Effective Mass

A number of experimental investigations have provided information about the dependence of the conduction-band effective mass upon electron concentration in HgSe. Room-temperature results were obtained by Wright, Strauss, and Harman[3] using infrared reflectivity and magnetoreflectivity

measurements. Shalyt and Aliev[4] used Hall-effect and thermoelectric-power measurements in strong magnetic fields to determine the dependence of the electron effective mass on concentration in the liquid-nitrogen–temperature region. Similar measurements were employed by Aliev, Korenblut, and Shalyt[5] to extend the results to temperatures between 95 and 300 °K. In the liquid-helium–temperature region, only one investigation of this kind has been reported. Using the temperature dependence of the amplitudes of Shubnikov–de Haas (SdH) oscillations, Whitsett[2] determined the cyclotron effective masses of the conduction electrons at the Fermi surface for samples having from 1.86×10^{17} to 4.52×10^{18} electrons/cm^3.

In the above studies, a nonparabolic conduction-band model derived by Kane[6] for InSb was found to account satisfactorily for the effective-mass variation. By comparing their data with the nonparabolic conduction-band model, the above authors obtained values of E_g, the forbidden energy gap at $k=0$, and P, the momentum matrix element between conduction- and valence-band Bloch functions at $k=0$.[7] Harman[8] reanalyzed the data taken by Wright *et al.*[3] and obtained values of P and E_g different from those originally reported. Values of P and E_g slightly different from either those obtained by Wright *et al.*, Whitsett, or Harman, were reported by Bliek and Landwehr[9] (see Ref. 10 for listing of the parameters used in calculations in Ref. 9), who reanalyzed the published electron effective-mass data of Wright *et al.*[3] and Whitsett.[2]

There are several reasons why the simple Kane model used in these cases is not applicable to the conduction band in HgSe. First, the expression for the conduction-band energy that was employed is valid only if the spin-orbit splitting Δ of the valence bands is much larger than E_g. Bliek and Landwehr[10] have shown that this may not be a good assumption for HgSe. Second, the effect of higher-band $\vec{k}\cdot\vec{p}$ interactions on the effective mass were not considered. In the case of HgTe, Groves, Brown, and Pidgeon[11] showed that the assumptions of infinite spin-orbit splitting and of no interactions with higher bands (usually made in the m^*-vs-n analysis for E_g and P) can cause serious errors for a Γ_8 conduction band. (Bliek and Landwehr[10] did not include the effects of higher bands in their analysis.) Third, the recent study of the SdH effect at liquid-helium temperatures by GSB has confirmed that the conduction band in HgSe has Γ_8 symmetry, as in HgTe. Therefore, the conduction-band model of Γ_6 symmetry, as in InSb, is not, strictly speaking, applicable.

In this paper, we calculate the concentration dependence of the cyclotron resonance effective mass for a band model which takes into account the effects of finite spin-orbit splitting and higher-band interactions for a Γ_8 conduction band, as in HgSe. The energy-band parameters needed in this calculation are adjusted to give a good fit not only to Whitsett's SdH effective-mass data, but also to the previously reported SdH frequency anisotropy results of GSB. In addition, our theoretical analysis gives values for the effective-mass anisotropy and its concentration dependence.

B. Beating Effects in SdH Oscillations in HgSe

Beating effects have been observed in the SdH oscillations by Whitsett[2] in the II-VI semiconductor HgSe, and in the III-V semiconductor GaSb by Seiler *et al.*[12,13] For both materials, the beating is found to be associated with the carriers in the $k=0$ conduction-band minimum. Whitsett[2] proposed that although the Fermi surface of the conduction band is nearly spherical in HgSe, the beating effects may arise because of slight bulging of the Fermi surface in the $\langle111\rangle$ directions in k space. Such a model implies that two extremal cross sections perpendicular to the magnetic field may have different areas for certain field directions, thus leading to the observed beating. Groves and Wyatt[14] considered the possibility of obtaining beating effects from two extremal orbits on a warped Fermi surface; from Whitsett's measurements of the anisotropy of the SdH period they concluded that the size of the warping expected in HgSe is much smaller than that needed to produce the observed beating.

Roth, Groves, and Wyatt,[15] and Roth[16] have shown that inversion asymmetry effects appearing in zinc-blende structures produce two orbits for carriers in the conduction band of HgSe and lead to the orientation-dependent beating observed by Whitsett in this material. Seiler, Becker, and Roth[13] demonstrated that the beating behavior seen in GaSb is not simple and thus cannot be fully explained in terms of a semiclassical model of two Fermi surfaces produced by inversion asymmetry splitting. The authors showed that the quantum-mechanical theory of Roth which includes the interaction between the electron spin and external magnetic fields accounts for many of the major features of the GaSb data.

In the case of GaSb, the beating effects can be detected only for a rather narrow concentration range [$n=(1.2\text{–}1.5)\times10^{18}$ cm^{-3}]. Although Whitsett observed beating in HgSe over a wide concentration range, detailed investigation was carried out only for a sample with $n\sim1.3\times10^{18}$ cm^{-3}. Thus, in both semiconductors, data are lacking on the concentration dependence of the beating effects. In HgSe, improved crystal growth technology, increased understanding of the band structure, and the existence of a successful theoretical model to explain the beating effects suggests that a wider and more extensive investigation than had been undertaken by

Whitsett should be considered for this material.

In this paper, we present detailed observations of beating effects in the SdH oscillations in HgSe. Sample behavior was investigated in the electron concentration range from 4.69×10^{17} to 3.73×10^{18} cm^{-3}. Systematic studies of (i) the concentration dependence of nodal positions, and (ii) the variation of nodal positions with magnetic field direction are reported. It will be shown that certain features of the beating behavior cannot be explained in terms of a semiclassical model of two Fermi surfaces produced by inversion asymmetry splitting of the $k=0$ conduction band. Although many of the earlier experimental results in HgSe have already been explained by the quantum-mechanical theory of Roth *et al.*[15] and Roth,[16] understanding of some of the new results given below will require further development of the theory.

II. THEORY

Earlier, Roth, Groves, and Wyatt[15] estimated the size of the zinc-blende splitting in HgSe from Whitsett's data by assuming a semiclassical model. In their paper, an E-vs-k relation derived by Kane,[6] good for either Γ_6 or Γ_8 band symmetry, was used to calculate the area difference between the two extremal cross-sectional areas of the Fermi surface which are perpendicular to the magnetic field direction. The size of the band parameter β (Kane's B) depends on the choice of band symmetry and is related to the splitting; Roth, Groves, and Wyatt[15] estimated the size of β for both symmetries. GSB showed from the concentration dependence of the angular anisotropy of the SdH effect, that the $k=0$ conduction-band minimum in HgSe has Γ_8 symmetry. Roth, Groves, and Wyatt[15] carried out their calculations by computer techniques. Seiler and Becker[17] had found that in GaSb the SdH period exhibits dependencies on magnetic field direction of a simple functional form. Starting with an E-vs-k equation involving nonparabolicity and warping, they were able to develop by analytical methods expressions for the extremal cross-sectional area, and thus the SdH period, which exhibited the same functional forms, thus allowing direct comparison with experiment. Seiler, Becker, and Roth[13] outlined a similar calculation for GaSb which in addition to the nonparabolicity and warping, also takes into account the energy contribution due to inversion asymmetry splitting. Recently, we completed an analysis of the warping and symmetry of the conduction band in HgSe from SdH measurements[1] using the analytical methods of Seiler and Becker.[17] (A description of this calculation is given in the Appendix of the present paper, together with the extension of this analysis to include inversion asymmetry splitting.) It is shown in the Appendix that, to a reasonable approximation,

$$k_{\rho\pm}^2 \approx C_0[1 - C_1 y_1(\theta,\varphi) \mp C_2 y_2(\theta,\varphi)], \tag{1}$$

where

$$C_0 = \frac{2m_0}{\hbar^2}\,\frac{(E^{\pm})^2 - E^{\pm}E_g}{Z}\,, \tag{2}$$

$$C_1 = v\,\frac{2E^{\pm}(1+k_F^2P^2/3\Delta^2) - (E_g + k_F^2P^2/3\Delta)}{Z}\,, \tag{3}$$

$$C_2 = w\,\frac{2E^{\pm}(1+k_F^2P^2/3\Delta^2) - (E_g + k_F^2P^2/3\Delta)}{Z}\,, \tag{4}$$

and

$$Z = \frac{(\frac{2}{3}+\gamma)P^2 - E^{\pm}P^2/3\Delta^2 + E^{\pm}P^2/3\Delta}{\hbar^2/2m_0} + u[2E^{\pm}(1+k_F^2P^2/3\Delta^2) - (E_g + k_F^2P^2/3\Delta)]. \tag{5}$$

Here $E^{\pm}$ is the Fermi energy, E_g is the direct energy gap at $k=0$, P is the momentum matrix element, Δ is the energy splitting of the valence band due to spin-orbit interaction, m_0 is the free-electron mass, and γ is a small term which depends upon concentration. (For infinite spin-orbit splitting, $\gamma=0$.) For HgSe, we note that $E_g<0$. $k_{\rho\pm}$ and φ are a set of polar coordinates lying in the plane perpendicular to the magnetic field $\vec{B}$, and θ is the angle between the field direction and a crystallographic direction lying in the plane of rotation of the magnetic field. The form of the functions $y_1(\theta,\varphi)$ and $y_2(\theta,\varphi)$ depends on the plane of rotation of the magnetic field. Seiler and Becker[17] give the form of $y_1(\theta,\varphi)$ for $\vec{B}$ lying in a (110) plane and Seiler, Becker, and Roth[13] give the form of $y_2(\theta,\varphi)$ for the same field orientation. The coefficients u, v, and w are defined in the Appendix; they contain the effects of the higher-band interactions.

In Eqs. (2)–(4), k_F is an appropriate spherical k vector. The coefficients C_0, C_1, and C_2 are only dependent on the Fermi energy and the band parameters; their evaluation is outlined in the Appendix. The extremal cross-sectional areas $\mathfrak{a}_{\pm}$ perpendicular to the magnetic field are given by

$$\mathfrak{a}_{\pm} = \pi C_0[1 - (C_1/2\pi)g_1(\theta) \mp (C_2/2\pi)g_2(\theta)]. \tag{6}$$

The function

$$g_1(\theta) = \int_0^{2\pi} y_1(\theta,\varphi)\,d\varphi$$

is evaluated in Appendix A of Ref. 17 for $\vec{B}$ lying in the (110) plane. The integral

$$g_2(\theta) = \int_0^{2\pi} y_2(\theta,\varphi)\,d\varphi$$

is given in Ref. 13, also for the case where $\vec{B}$ lies in the (110) plane.

A. Effective-Mass Calculations and Analysis

The cyclotron effective mass is defined as[18]

$$m^* = \frac{\hbar^2}{2\pi}\,\frac{d\mathfrak{a}}{dE}\,, \tag{7}$$

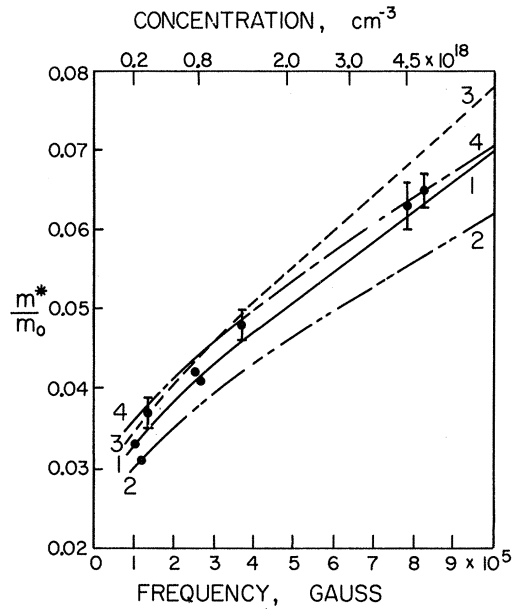

FIG. 1. Variation of cyclotron effective mass as a function of SdH frequency. The data points, along with their uncertainties, were obtained from Ref. 2. The curves show the results of calculations using the following sets of band parameters: curve 1 (results of present calculation), $P=7.2\times10^{-8}$ eV cm, $E_g=-0.22$ eV, $\Delta=0.45$ eV, $A'=0$, $M=-5$, $L'=-2$, and $(L-M-N)=4$; curve 2 (higher-band parameters set equal to zero), $P=7.2\times10^{-8}$ eV cm, $E_g=-0.22$ eV, $\Delta=0.45$ eV, and $A'=M=L'=(L-M-N)=0$; curve 3 (obtained from Ref. 10 and including the higher-band interactions), $P=6.6\times10^{-8}$ eV cm, $E_g=-0.19$ eV, $\Delta=0.38$ eV, $A'=0$, $M=-5$, $L'=-2$, and $(L-M-N)=4$; curve 4 (obtained from Ref. 2 and including the higher-band interactions), $P=7.1\times10^{-8}$ eV cm, $E_g=-0.24$ eV, $\Delta=0.45$ eV, $A'=0$, $M=-5$, $L'=-2$, and $L-M-N=4$.

where $\mathfrak{a}$ is the area of the Fermi surface in the $\vec{k}_H=0$ plane (where $\vec{k}_H$ is parallel to the magnetic field direction), m^* is the cyclotron mass when the magnetic field is along the $\vec{k}_H$ direction, and E is the Fermi energy. The derivative in Eq. (7) can be conveniently determined numerically by finding the appropriate E and $\mathfrak{a}$ for slightly different values of concentration or k vector and then taking the quotient of the differences. In calculating the effective mass, we neglect the influence of the inversion asymmetry splitting term by setting $C_2=0$. This should be a good approximation since the energy splitting is small.

1. *Extraction of Band Parameters from Whitsett's Data*

Whitsett's effective-mass data are presented in Fig. 1. The SdH frequencies in the figure are calculated from the $\vec{B}\|\langle100\rangle$ period data at 4.2 °K given in Table II of Whitsett's paper.[2] Values of the effective masses for $\vec{B}\|\langle100\rangle$ are taken from Table IV of the same reference. The possible experimental error in the SdH periods or frequencies is ± 5%, according to Whitsett. A measure of the uncertainty in Whitsett's m^* data can be obtained from the scatter of mass values computed for several magnetic field strengths from the average value; Whitsett estimated these to be of the order ± 0.001 or less. The uncertainties in Whitsett's data are indicated by the error bars in Fig. 1.

A good fit to the experimental data is obtained assuming the following set of band parameters: $P=7.2\times10^{-8}$ eV cm, $E_g=-0.22$ eV, $\Delta=0.45$ eV, $A'=0$, $B'=0$, $M=-5$, $L'=-2$, and $L-M-N=4$. (The higher-band parameters are given in units of $\hbar^2/2m_0$.) This same set of parameters has previously been shown to give an excellent fit to recent data on the concentration dependence of the magnitude of the warping of the Fermi surface in HgSe.[1] Although the separate fittings do not necessarily give a unique set, the values chosen can be considered as reasonable, based on present knowledge of the band parameters in cubic semiconductors. More recently, Broerman has used this set of band-parameter values in an analysis of the concentration dependence of the Hall mobility in n-HgSe at 4.2 °K.[19] To illustrate how significant the omission of the higher-band parameters can be to the effective-mass calculation, we also show in Fig. 1 the computed results using both Whitsett's[2] and Bliek and Landwehr's band parameters,[9,10] together with the above-assumed values of the higher-band parameters.

Table I lists the values of the band parameters P and E_g obtained from a variety of investigations together with the corresponding band-structure assumptions used in the analysis of the data.

2. *Anisotropy of Effective Mass*

Since the Fermi surface is slightly nonspherical, the effective mass is slightly anisotropic. The angular dependence of the cyclotron effective mass is given by the function $g_1(\theta)$, as seen from Eqs. (6) and (7). Calculation of this angular dependence is shown in Fig. 2 for a sample with an electron concentration of $\approx 1.6\times10^{18}/\text{cm}^3$. The magnitude of this anisotropy depends upon concentration in the manner presented in Fig. 3.

B. Beating Effects

If inversion asymmetry is included in the evaluation of $\mathfrak{a}$ in Eq. (6), then the SdH frequencies contributed by the two areas are

$$F_{\pm}(\theta)=\frac{\hbar c C_0}{2e}\left(1-\frac{C_1}{2\pi}g_1(\theta)\mp\frac{C_2}{2\pi}g_2(\theta)\right). \tag{8}$$

Thus, the semiclassical result for the beat frequency, given by this calculation, is

$$F_B=F_0(C_2/\pi)g_2(\theta), \tag{9}$$

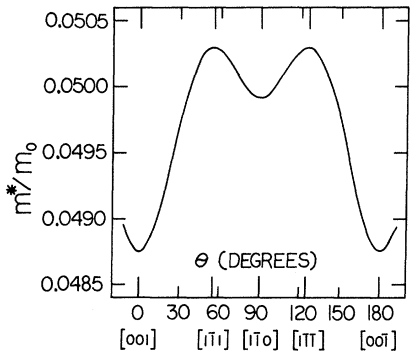

FIG. 2. Angular variation of the effective mass for an electron concentration $n \sim 1.6\times10^{18}/\mathrm{cm}^3$.

where $F_0=\hbar c C_0/2e$ is the SdH frequency obtained by ignoring both inversion asymmetry and warping. The number of oscillations between nodes is F_0/F_B. In Eq. (9), the concentration dependence of the beat frequency is in the C_0C_2 product, and the angular dependence is given by the $g_2(\theta)$ function.

As in the case of Whitsett, we observe two nodal points for limited angular ranges around $\vec{B}\|\langle 111\rangle$, but only one nodal point for $\vec{B}\|\langle 100\rangle$. Where two nodal points are seen, we calculate the beat frequency from the data according to the expression

$$F_B=[(1/B_{\text{node }1}-1/B_{\text{node }2})]^{-1} \tag{10}$$

for comparison with the theory.

TABLE I. Comparison of values of P and E_g obtained from analysis of effective-mass data on HgSe.

P(eV cm)	$\lvert E_g\rvert$ (eV)	Ref.	Comments
8×10^{-8}	~ 0.2	3	Large Δ, no higher bands; obtained from room-temperature reflectivity data assuming Γ_6 energy band.
7.1×10^{-8}	0.24	2	Large Δ, no higher bands; obtained from oscillatory magnetoresistance data taken at liquid-helium temperature assuming Γ_6 energy band.
7.62×10^{-8}	0.2	9	Large Δ, no higher bands; obtained from published data assuming Γ_6 energy band.
7.5×10^{-8}	0.15	8	Large Δ, no higher bands; reanalysis of data from Ref. 3.
6.6×10^{-8}	0.19	10	Finite Δ, no higher bands; obtained from analyzing data on Ref. 2 assuming a Γ_8 energy band.
7.2×10^{-8}	0.22	This paper	Finite Δ, higher bands included; obtained from analyzing data of Refs. 2 and 1. Γ_8 symmetry of the conduction band was confirmed by the authors in Ref. 1 and thus a Γ_8 energy band must be used.

III. EXPERIMENTAL

Experimental techniques connected with the SdH measurements have been described by Seiler and Becker, [17] and details on sample preparation were presented in GSB. In Fig. 4 (taken from Ref. 1), we show typical data for several field directions transverse to the current direction. For $\vec{B}\|[001]$, the nodal position is easily established by inspection to within one cycle of the SdH oscillation. For $\vec{B}\|[111]$, the low-field nodal position can also be clearly seen. In the case of the high-field nodal position for this field orientation, however, the large harmonic content of the oscillation introduces a considerable uncertainty in the determination of the amplitude minimum. (This latter point will be further discussed.) We investigated the dependence of nodal position on electron concentration in the range 4.69×10^{17} to 3.73×10^{18} cm^{-3} for the magnetic field directions $\vec{B}\|\langle 111\rangle$ and $\vec{B}\|\langle 100\rangle$. We also studied the angular variation of the nodal positions for the transverse orientation ($\vec{I}\perp\vec{B}$) for the cases $\vec{I}\|\langle 100\rangle$ and $\vec{I}\|\langle 110\rangle$. Table II lists the electrical properties of the samples together with the respective nodal positions of the beats for $\vec{B}\|\langle 111\rangle$ and $\vec{B}\|\langle 100\rangle$. The corresponding Landau-level numbers are given in parentheses. No beating effects were observed for $\vec{B}\|\langle 110\rangle$.

Figure 5 summarizes the data on the nodal positions. Whitsett's measurements are presented on the same plot. The nodal point positions were first surveyed in dc magnetic fields up to 20 kOe using a

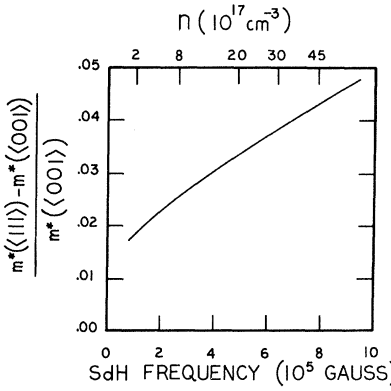

FIG. 3. The magnitude of the effective-mass anisotropy (plotted as $[m^*(\langle 111\rangle)-m^*(\langle 001\rangle)]/m^*(\langle 001\rangle)$) as a function SdH frequency. For convenience, the electron concentration is also indicated. [The symbol $m^*(\langle hkl\rangle)$ denotes the effective mass with the magnetic field aligned along the given crystallographic direction.]

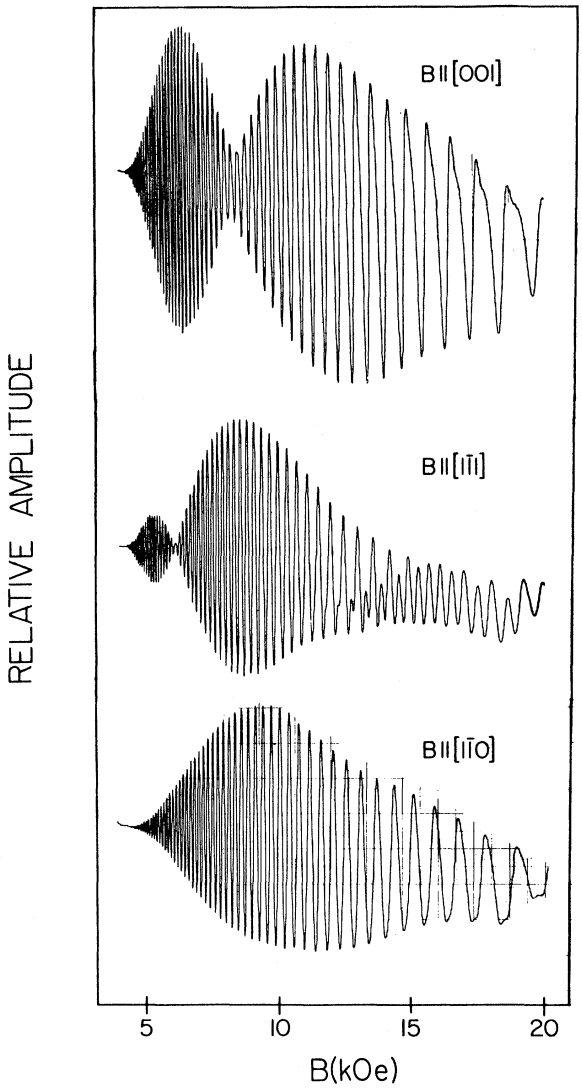

FIG. 4. Reproduction of x-y recorder traces of oscillatory magnetoresistance data taken on sample 4a at 1.3 °K using field-modulation and phase-sensitive detection techniques. The signal is obtained while detecting at the second harmonic of the modulation frequency. This figure is taken from Ref. 1, Fig. 3.

4-in. Pacific Electric Motor electromagnet. For the highest-concentration samples, it was necessary to employ an 80-kOe Westinghouse superconducting magnet to see the $\vec{B}\parallel\langle 111\rangle$ high-field nodal point.

Figure 6 shows the variation of the nodal positions with magnetic field direction in sample 4aT for $\vec{B}\perp\vec{I}\parallel\langle 110\rangle$. As seen in the figure, no beating is found for $22^\circ < \theta < 35^\circ$. Figure 7 gives the x-y recorder trace corresponding to the field direction $\theta = 25^\circ$ in Fig. 6. At ~ 30° and 90°, the amplitude dependence on field is observed to be quite similar in appearance. The behavior for $\vec{B}\perp\vec{I}\parallel\langle 110\rangle$ observed in sample 4aT appears to be typical.

A different angular variation is seen in Fig. 8 for the current-field orientations $\vec{B}\perp\vec{I}\parallel\langle 100\rangle$ in sample 16a. Among the samples listed in Table II, only 16a had the correct orientation for this study.

As seen in Fig. 4, the oscillatory frequency appears to be doubled in the region of the high-field nodal point for $\vec{B}\parallel\langle 111\rangle$. In our data, the oscillations are usually obtained using field modulation and phase-sensitive detection techniques. This frequency doubling is also observed using dc methods. We assume that the doubling shows the presence of the second harmonic of the SdH frequency. The maximum amplitude of the second harmonic should then appear at the minimum amplitude of the first harmonic (the first harmonic is the fundamental SdH frequency); this field point was taken as the high-field nodal position. As a check, it is seen that the component identified as the second harmonic is damped more than the first harmonic as the temperature increases, as expected. The nodal position obtained from the high-temperature minimum in the first harmonic is in good agreement with the same position obtained from the low-temperature maximum in the second harmonic.

We note that for $\vec{B}\parallel\langle 111\rangle$, the amplitude is very close to zero at the low-field nodal position. For $\vec{B}\parallel\langle 100\rangle$, however, the amplitude is still quite large at the nodal position, but no second harmonic structure is seen. Data for a low-concentration sample 7a, showing this latter feature of the beating for $\vec{B}\parallel\langle 100\rangle$, are presented in Fig. 9.

IV. RESULTS AND DISCUSSION

Table I of Roth's paper[16] lists the nodal points observed by Whitsett for three samples of concentra-

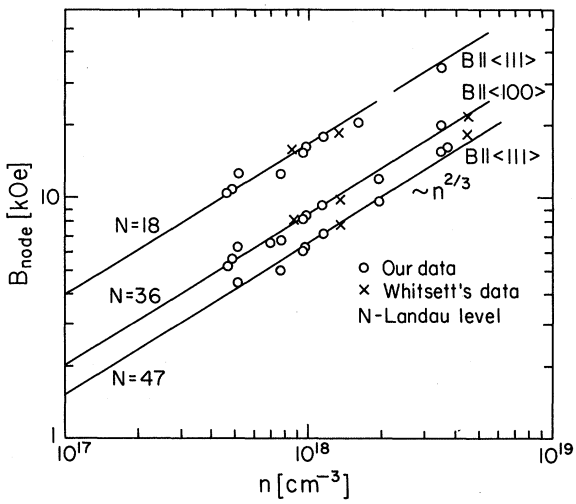

FIG. 5. Concentration dependence of the nodal positions for current orientation $\vec{I}\parallel\langle 110\rangle$ and magnetic field orientations $\vec{B}\parallel\langle 111\rangle$ and $\vec{B}\parallel\langle 100\rangle$. Slope of the straight lines drawn through the data points is $\frac{2}{3}$.

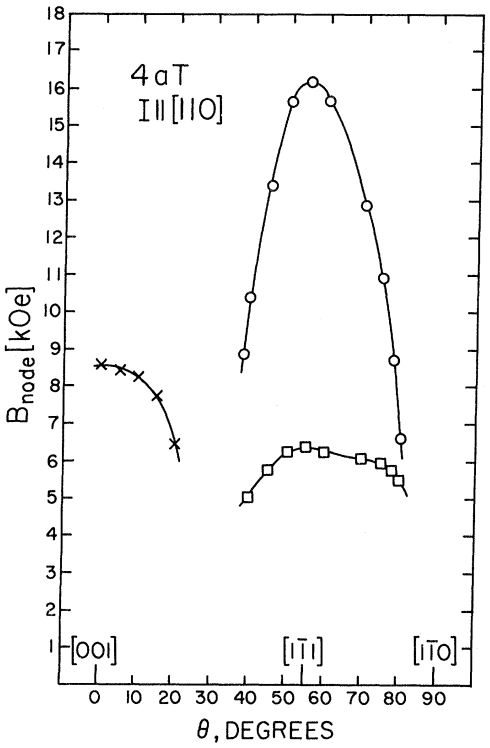

FIG. 6. Variation of the nodal positions with magnetic field direction for $\vec{B} \perp \vec{I} \parallel [100]$.

tion 8.46×10^{17}, 1.34×10^{18}, and 4.52×10^{18} cm^{-3}. These same results are included in the data presented in Fig. 5. Roth[16] has suggested that shifts in Landau-level number of the nodes with concentration may be related to changes in both the quantities μ and γ (our C_2). In Roth's theory, we have

$$\mu = \tfrac{1}{2}(1 - \omega_s/\omega_c) = \tfrac{1}{2}(1 - gm^*/2m_0),$$

where ω_c is the cyclotron resonance frequency, and g is the spin-splitting factor. *Inspection of Fig. 5 shows that to within the accuracy of the measurements, the Landau-level numbers of the nodal positions for* $\vec{B} \parallel \langle 111 \rangle$ *and* $\vec{B} \parallel \langle 100 \rangle$ *are independent of carrier concentration.* Both μ and γ would be expected to change with concentration in a complicated band. The absence of any shifts in Landau-level number suggests that any changes in these quantities which do occur (i) are small, or (ii) compensate each other. The constancy of the nodal positions is not inconsistent with predictions of the semiclassical theory, since predictions relating only to the beat frequency are given by this theory.

Roth[16] has obtained a value of $C_2 = 0.085$ from a fit to Whitsett's data for a sample with $n = 1.34\times10^{18}$ cm^{-3}. According to the earlier work on this problem, [15] this value of C_2 corresponds to a value of β of 6.52 (in units of $\hbar^2/2m_0$). (We assume Γ_8 symmetry and use appropriate values of a and b in deriving this latter result.) Assuming that the two nodal points for $\vec{B} \parallel \langle 111 \rangle$ represent simple beating, we find from the semiclassical analysis given in Sec. II B of this paper a value of $C_2 = 0.045$ and a corresponding value of $\beta = 3.45$ (in units of $\hbar^2/2m_0$) in a sample with $n = 1.34\times10^{18}$ cm^{-3}.

In order to derive the above values of β, we have employed the following band parameters: $E_g = -0.22$ eV, $P = 7.2\times10^{-8}$ eV cm, $\Delta = 0.45$ eV, and $A' = 0$, $M = -5$, $L' = -2$, and $(L - M - N) = 4$ in units of $\hbar^2/2m_0$. This dissimilarity between the values of β derived

TABLE II. Summary of samples investigated for beating effects. The Landau-level numbers of the nodal positions are calculated from $N = (B_N P)^{-1}$, where B_N is the magnetic field at which the node is observed, and P is the SdH period. In the table, the value of N is given in parentheses. For $\vec{B} \parallel \langle 111 \rangle$, $N_{\text{higher field}} = 18 \pm 1$ and $N_{\text{lower field}} = 47 \pm 1$. For $\vec{B} \parallel \langle 100 \rangle$, $N = 36 \pm 1$.

Sample	$n = 1/R_H e$ (cm^{-3})	σ (Ω cm)$^{-1}$	$R_H\sigma$ (cm^2/V sec)	Nodal positions $\vec{B} \parallel \langle 111 \rangle$ (kOe)		$\vec{B} \parallel \langle 100 \rangle$ (kOe)
7*a*	4.69×10^{17}	5.75×10^3	90.0×10^3	•••	10.5 (18)	5.25(36)
1*a*	4.88×10^{17}	5.775×10^3	74.3×10^3	•••	10.75(16)	5.60(30)
7*a T*[a]	6.08×10^{17}	9.90×10^3	95.4×10^3	4.5 (50)	12.7 (18)	6.30(36)
16*a*[b]	6.99×10^{17}	9.7×10^3	87.0×10^3	•••	•••	6.55(35)
15*a*	7.75×10^{17}	13.0×10^3	104.7×10^3	5.0 (50)	12.65(20)	6.70(37)
4*a*	9.50×10^{17}	10.5×10^3	69.0×10^3	6.1 (48)	15.5 (19)	8.30(35)
4*a T*[c]	9.69×10^{17}	11.2×10^3	72.5×10^3	6.35(47)	16.2 (18)	8.55(35)
1*aa*	11.5×10^{17}	12.36×10^3	66.9×10^3	7.2 (46)	18.0 (18)	9.40(35)
11*aa*	16×10^{17}	•••	•••	•••	20.8 (20)	•••
11*a*	19.6×10^{17}	17.57×10^3	56.2×10^3	9.7 (48)	•••	12 (39)
12*a*	35.0×10^{17}	24.9×10^3	44.7×10^3	15.8 (44)	•••	20 (39)
13*a*	37.3×10^{17}	25.25×10^3	42.2×10^3	16.2 (45)	34.8 (20)	•••

[a]Sample 7*a* remeasured after approximately 4 months room-temperature anneal.

[b]Sample with $\vec{I} \parallel \langle 100 \rangle$. All other samples were oriented with $\vec{I} \parallel \langle 110 \rangle$.

[c]Sample 4*a* remeasured after approximately 4 months room-temperature anneal.

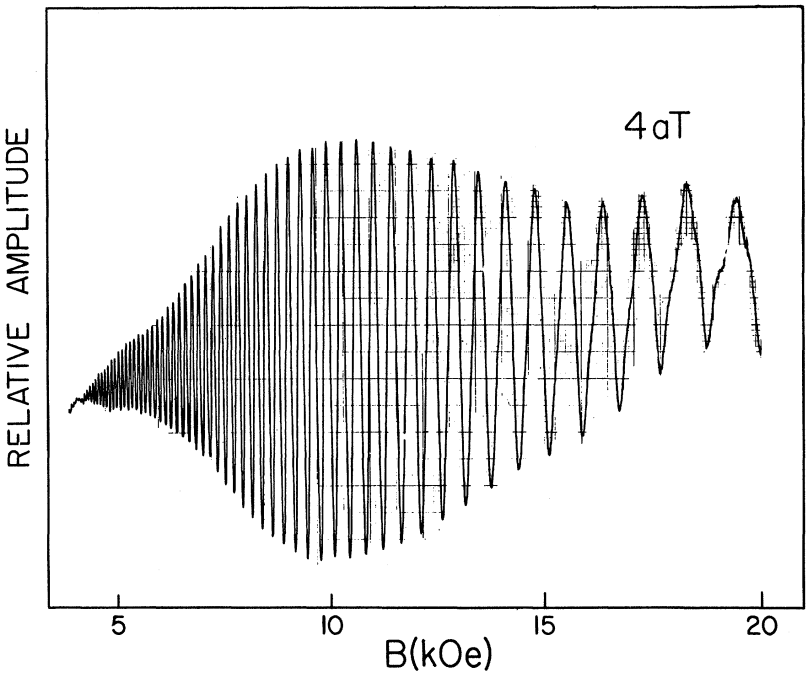

FIG. 7. Reproduction of x-y recorder trace of oscillatory magnetoresistance data taken on sample 4a T using field-modulation and phase-sensitive detection techniques. The monotonically changing magnetic field is parallel to a direction 30° away from [001] in the plane $\vec{B} \perp \vec{I} \parallel$ [110]. The signal is obtained while detecting at the second harmonic of the modulation frequency.

semiclassically and from the quantum theory has already been noted for the GaSb case.[13] As seen in Fig. 10, the concentration dependence of the beat frequency for $\vec{B} \parallel \langle 111 \rangle$ can be fitted with the value of $\beta = 3.45$ over the complete concentration range using the semiclassical theory.

Inspection of Fig. 6 shows that as the magnetic field is turned away from the $\langle 111 \rangle$ direction, toward the $\langle 110 \rangle$ direction, the two $\langle 111 \rangle$ nodal points approach each other. If the two nodes for $\vec{B} \parallel \langle 111 \rangle$ are connected by simple beating, more nodes should be seen in the field range of measurement for this direction of field rotation. No such additional nodes are detectable. A similar behavior of the nodal points has been noted in the case of GaSb and has been cited as evidence for the inadequacy of the semiclassical theory.[13]

The quantum-mechanical calculations of Roth[16] were made only for $\vec{B} \parallel \langle 100 \rangle$, $\vec{B} \parallel \langle 110 \rangle$, and $\vec{B} \parallel \langle 111 \rangle$. For other field directions, the Hamiltonian has not been solved as yet. Comparison between the results given in Fig. 6, and results obtained for the same orientation ($\vec{B} \perp \vec{I} \parallel \langle 110 \rangle$) in GaSb (see Fig. 12

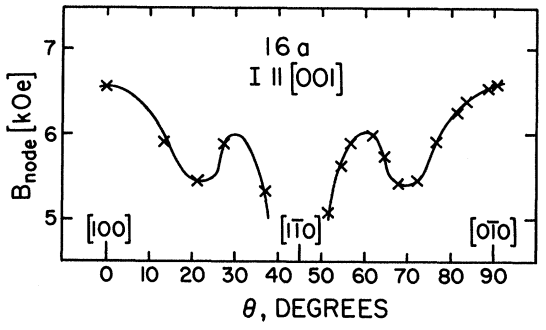

FIG. 8. Variation of the nodal position with magnetic field direction for $\vec{B} \perp \vec{I} \parallel$ [001].

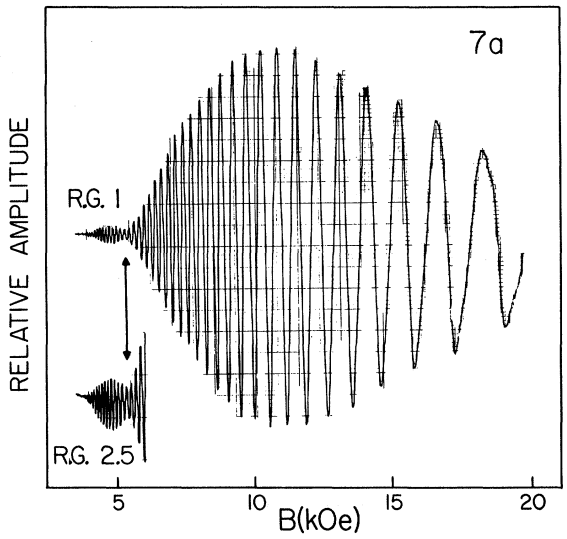

FIG. 9. Reproduction of x-y recorder trace of oscillatory magnetoresistance data taken on sample 7a using field-modulation and phase-sensitive detection techniques. The monotonically changing magnetic field is parallel to the [100] direction. RG indicates the relative gain employed in the measurements. The signal is obtained while detecting at the second harmonic of the modulation frequency.

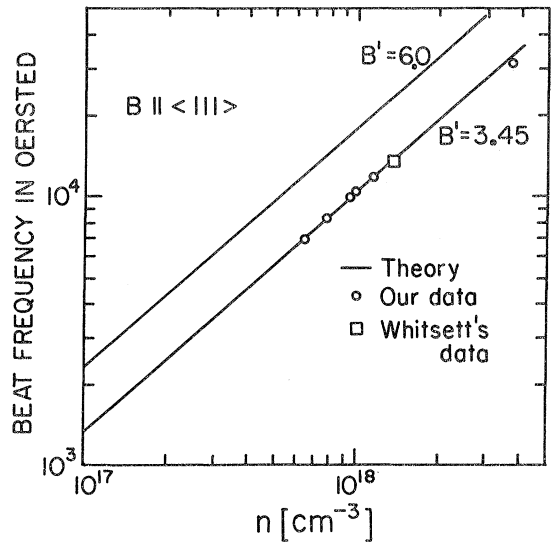

FIG. 10. Theoretical and experimental dependence of beat frequency on electron concentration for $\vec{B} \parallel \langle 111 \rangle$. The theoretical curves are obtained using the semiclassical theory outlined in the text. The experimental beat frequency is calculated from the data by assuming that the two observed nodes for $\vec{B} \parallel \langle 111 \rangle$ are related by simple beating. B' in the figure is the same as β (Kane's B) in the text.

in Ref. 13) shows that the angular behavior of the beating effects in these two semiconductors is quite similar. The similarity in results for GaSb and HgSe indicates that this aspect of the beating behavior may be a common feature of zinc-blende materials.

For $\vec{B} \parallel \langle 100 \rangle$, only one node has been observed so far (see Fig. 6). Our present results extend only to fields up to 80 kOe. Studies of the de Haas–van Alphen and Shubnikov–de Haas effects in n-HgSe in pulsed fields up to 210 kOe were carried out by Bliek and Landwehr[9] in samples with electron concentrations between 1.96 and 3.26×10^{18} cm^{-3}. These studies examined sample behavior only for the case $\vec{B} \parallel \langle 100 \rangle$. The results showed that no beating effects could be observed (except for the nodes previously found by Whitsett) at these high magnetic fields. Roth's theory predicts a weak minimum or "wobble" in the SdH amplitude at very high Landau-level numbers for the orientation $\vec{B} \parallel \langle 100 \rangle$; experimentally, it is found that the SdH oscillations are undetectable in the range of magnetic field strength corresponding to the position of this low-field minimum.

V. CONCLUSIONS

A new set of band parameters has been determined for HgSe from an analysis of previously published effective-mass data.

New results on the beating effects in the SdH oscillations in HgSe are reported. Calculations involving inversion asymmetry splitting indicate that the effects may be explained only in part using a semiclassical theory. The quantum-mechanical theory is as yet not complete enough to predict all the details of the observed behavior.

APPENDIX

A very useful presentation of the E-vs-k relationship for materials with diamond and zinc-blende lattices has been given by Kane.[6] Kane employed a perturbation theorem of Löwdin[20] to take into account bands far removed in energy from the lowest-lying conduction band and the highest-lying valence bands. These states at $k = 0$ are put into one of two groups: Group A includes the closely bunched states of interest (Γ_6, Γ_7, and Γ_8) and group B includes the remainder. Any state in group A interacts only weakly with any state in group B, but may interact strongly with any other state in group A. The $\vec{k} \cdot \vec{p}$ interactions between states in A and B are then removed to lowest order by ordinary perturbation theory which leaves the states in A with a "renormalized" interaction matrix which must be diagonalized exactly. Löwdin showed that

$$h'_{ij} = h_{ij} + \sum_{\beta}^{B} \frac{h_{i\beta} h_{\beta j}}{E_i - h_{\beta\beta}} , \tag{A1}$$

where h_{ij} is the initial interaction matrix and h'_{ij} is the "renormalized" matrix. In Eq. (A1), i, j are in A and β is in B. The warping and inversion asymmetry terms come from the second term in Eq. (A1).

The spin-orbit interaction plays an important role in the calculation of band structures. With spin considered, the combined action of the spin-orbit and $\vec{k} \cdot \vec{p}$ interactions leads to an 8×8 interaction matrix which can easily be diagonalized by machine calculations. This has been done by Bell and Rodgers[21] for the case of InSb. However, for analytic purposes a much simpler procedure uses Kane's "small gap" or "three-band approximation." In this approach, the $\vec{k} \cdot \vec{p}$ and spin-orbit interaction matrix [h_{ij} of Eq. (A1)] between the Γ_6, Γ_7, and Γ_8 bands is diagonalized and then the higher-band $\vec{k} \cdot \vec{p}$ interactions [second term in Eq. (A1)] are treated by first-order perturbation theory. Kane has thus found the energy for either a Γ_6 or a Γ_8 band to be of the following approximate form:

$$E^{\pm} = E' + u\hbar^2 k^2/2m_0 + v f_1(\vec{k})\hbar^2/2m_0 \pm w f_2(\vec{k})\hbar^2/2m_0 , \tag{A2}$$

where

$$u = 1 + a^2 A' + b^2 M + c^2 L' , \tag{A3}$$

$$v = (b^2 - 2c^2)(L - M - N) , \tag{A4}$$

$$w = \sqrt{2}\, abB' , \tag{A5}$$

$$f_1(\vec{k}) = (k_x^2k_y^2 + k_x^2k_z^2 + k_y^2k_z^2)/k^2, \quad \text{(A6)}$$

and

$$f_2(\vec{k}) = [k^2(k_x^2k_y^2 + k_x^2k_z^2 + k_y^2k_z^2) - 9k_x^2k_y^2k_z^2]^{1/2}/k. \quad \text{(A7)}$$

The conduction-band eigenvalue E' results from diagonalizing the Hamiltonian which includes the $\vec{k}\cdot\vec{p}$ and the largest spin-orbit interaction terms between an s-like (Γ_6) and p-like ($\Gamma_7+\Gamma_8$) basis. The normalized coefficient a gives the amount of s-like basis function in the conduction-band eigenvector and the normalized coefficients b and c give the amounts of different component p-like basis functions in the conduction-band eigenvector. For example, at $k=0$, $a=1$ and $b=c=0$ for a Γ_6 band, while for a Γ_8 band $a=0$, $b=\sqrt{\frac{1}{3}}$ and $c=\sqrt{\frac{2}{3}}$. The parameters A', L, M, N, L', and B' (Kane's B), written in units of $\hbar^2/2m_0$, represent the interaction between far-removed conduction- and valence-band edges and the s- and p-like bands. The term $f_1(\vec{k})$ produces a warping of the Fermi surface and the term $f_2(\vec{k})$ gives the inversion asymmetry splitting. For very small k, the energy goes as k^2, while for small k, the warping term adds energy terms of order k^4 and the inversion asymmetry splitting term adds terms of order k^3. The inversion asymmetry splitting term is not expected to affect the average SdH frequency. The experimental results show that only the warping term need be included to explain the observed anisotropy of the SdH frequency. For a Γ_8 band, there is also a splitting term linear in k, which we neglect.

Roth, Groves, and Wyatt[15] concluded that the maximum cross-sectional area perpendicular to the magnetic field occurs at $\vec{k}_H=0$ (where $\vec{k}_H$ is parallel to the magnetic field direction), since the angular anisotropy of the SdH oscillations observed by Whitsett in HgSe is small. The extremal cross-sectional area of the Fermi surface can be conveniently calculated by rotating the coordinate system so that the magnetic field, $\vec{B}$, is always parallel to one of the new coordinate axes. The details of this transformation are described in Appendix A of Ref. 17 and are here briefly summarized. The functions $f_1(\vec{k})$ and $f_2(\vec{k})$ are defined by $f_1(\vec{k}) = k_\rho^2 y_1(\theta, \varphi)$, and $f_2(\vec{k}) = k_\rho^2 y_2(\theta, \varphi)$, where k_ρ and φ are a set of polar coordinates lying in the plane perpendicular to $\vec{B}$, and θ is the angle between $\vec{B}$ and a cube axis. The form of these functions depends on the plane of rotation of the magnetic field.

The secular equation for Kane's "three-band approximation" is

$$(E'-E_c)(E'-E_v)(E'-E_v+\Delta) - k^2P^2(E'-E_v+\tfrac{2}{3}\Delta) = 0, \quad \text{(A8)}$$

where E' is the energy eigenvalue, Δ is the energy splitting of the valence band due to the spin-orbit interaction, and P is the momentum matrix element. If we take the energy zero at the top of the valence band (when $k=0$), $E_v=0$ and $E_c=E_g$, and Eq. (A8) may be rewritten as

$$(E'-E_g)(E') - k^2P^2(E'+\tfrac{2}{3}\Delta)/(E'+\Delta) = 0. \quad \text{(A9)}$$

Rewriting Eq. (A2) gives

$$E^{\pm} = E' + u\hbar^2k_{\rho\pm}^2/2m_0 + v\,y_1(\theta,\varphi)\hbar^2k_{\rho\pm}^2/2m_0 \pm w y_2(\theta,\varphi)(\hbar^2k_{\rho\pm}^2/2m_0). \quad \text{(A10)}$$

If the band parameters and Fermi energy are known, Eq. (A10) may be inverted to give $k_{\rho\pm}^2(\theta,\varphi)$ as a function of $E^{\pm}$ using numerical techniques. However, by using reasonable approximations we can rewrite Eq. (A10) in a form which avoids these extremely tedious calculations. The first step involves an approximation for the solution of Eq. (A9). This approximation is then introduced into Eq. (A10). The most important approximation we consider is the introduction, where appropriate, of a spherical k vector in the evaluation of various terms in both Eqs. (A9) and (A10). Algebraic manipulation then leads to an analytical relation between $k_{\rho\pm}^2$ and $E^{\pm}$, the Fermi energy. Finally, analytic expressions for the extremal cross-sectional area of the Fermi surface and the SdH period are obtained by integration of $k_{\rho\pm}^2$.

Since the conduction band has Γ_8 symmetry, the band structure of HgSe should have the inverted band structure of gray tin. Here E_g must be less than zero to satisfy Eq. (A9). Since $E'/\Delta < 1$, it is convenient to express Eq. (A9) in an approximate form for the E' solution for the Γ_8 conduction band. We note that

$$\frac{E'+\frac{2}{3}\Delta}{E'+\Delta} = 1 - \frac{1}{3(1+E'/\Delta)} \approx \frac{2}{3} + \frac{1}{3}\left[\frac{E'}{\Delta} - \left(\frac{E'}{\Delta}\right)^2 + \left(\frac{E'}{\Delta}\right)^3 - \left(\frac{E'}{\Delta}\right)^4 + \left(\frac{E'}{\Delta}\right)^5 - \left(\frac{E'}{\Delta}\right)^6 + \cdots\right]. \quad \text{(A11)}$$

To achieve an analytic expression for k_ρ^2, we approximate the cubic root of E' in Eq. (A9) by a quadratic root using a slowly varying parameter γ. In evaluating γ, we use the exact cubic solution E_e', for an appropriate spherical radius vector k_F, as outlined in Appendix B of Ref. 17. Thus

$$\gamma = \frac{1}{3}\left(\frac{E_e'}{\Delta}\right)\left[1 - \left(\frac{E_e'}{\Delta}\right) + \left(\frac{E_e'}{\Delta}\right)^2 - \left(\frac{E_e'}{\Delta}\right)^3 + \cdots\right] = \frac{1}{3}\left(\frac{E_e'}{\Delta}\right)^3 \frac{1}{1+E_e'/\Delta}. \quad \text{(A12)}$$

Equation (A9) can then be rewritten as

$$(E'-E_g)(E') - k^2P^2\left(\tfrac{2}{3}+\gamma+E'/3\Delta - E'^2/3\Delta^2\right) = 0. \quad \text{(A13)}$$

The solution of this quadratic equation corresponding to the Γ_8 conduction band is then

$$E' = \left\{\left(E_g + \frac{k_{\rho\pm}^2 P^2}{3\Delta}\right) + \left[\left(E_g + \frac{k_{\rho\pm}^2 P^2}{3\Delta}\right)^2 + 4\left(\tfrac{2}{3}+\gamma\right)k_{\rho\pm}^2 P^2 \times \left(1 + \frac{k_{\rho\pm}^2 P^2}{3\Delta^2}\right)\right]^{1/2}\right\} \Big/ 2\left(1 + \frac{k_{\rho\pm}^2 P^2}{3\Delta^2}\right) . \quad \text{(A14)}$$

After substituting Eq. (A14) into (A10), we obtain the Fermi energy

$$E_F = \left[2\left(1 + \frac{k_{\rho\pm}^2 P^2}{3\Delta^2}\right)\right]^{-1} \left\{\left(E_g + \frac{k_{\rho\pm}^2 P^2}{3\Delta}\right) + \left[\left(E_g + \frac{k_{\rho\pm}^2 P^2}{3\Delta}\right)^2 + 4\left(\tfrac{2}{3}+\gamma\right)k_{\rho\pm}^2 P^2 \left(1 + \frac{k_{\rho\pm}^2 P^2}{3\Delta^2}\right)\right]^{1/2} + u\frac{\hbar^2 k_{\rho\pm}^2}{2m_0} + v\, y_1(\theta, \varphi)\frac{\hbar^2 k_{\rho\pm}^2}{2m_0} \pm w y_2(\theta, \varphi)\frac{\hbar^2 k_{\rho\pm}^2}{2m_0}\right\} . \quad \text{(A15)}$$

After some algebraic manipulations, it can be shown that an approximate expression for $k_{\rho\pm}^2$ is

$$k_{\rho\pm}^2 = \frac{E_F^2 - E_g E_F}{Z} \Big/ \left(1 + \frac{[2E_F(1 + k_F^2 P^2/3\Delta^2) - (E_g + k_F^2 P^2/3\Delta)][v y_1(\theta, \varphi) \pm w y_2(\theta, \varphi)]}{Z}\right), \quad \text{(A16)}$$

where

$$Z = \frac{(\frac{2}{3}+\gamma)P^2 - E_F^2 P^2/3\Delta^2 + E_F P^2/3\Delta}{(\hbar^2/2m_0)} + u\left[2E_F\left(1 + \frac{k_F^2 P^2}{3\Delta^2}\right) - \left(E_g + \frac{k_F^2 P^2}{3\Delta}\right)\right] . \quad \text{(A17)}$$

Since the last term in the denominator is $\ll 1$, $k_{\rho\pm}^2$ is readily expanded and yields the expression

$$k_{\rho\pm}^2 \approx C_0[1 - C_1 y_1(\theta, \varphi) \mp C_2 y_2(\theta, \varphi)]; \quad \text{(A18)}$$

the functions C_0, C_1, and C_2 are given as Eqs. (2)–(4) in Sec. II.

The evaluation of the coefficients C_0, C_1, and C_2 starts with a value of k_F [or electron concentration, from which $k_F = (3n\pi^2)^{1/3}$]. The value of E_e' [used in evaluating γ] and the values of a, b, and c, are calculated for the Γ_8 band of HgSe in manner analogous to that presented in Appendix B of Ref. 17. Following Groves *et al.*,[11] we calculate the Fermi energy E_F by assuming $k_{\rho\pm} \approx k_F$, and use a spherical average of 0.1 k_F^2 for $f_1(\vec{k})$, thus

$$E_F = E_e' + (u + 0.1v)\hbar^2 k_F^2/2m_0 . \quad \text{(A19)}$$

Equations (A3)–(A5) are used to determine u, v, and w from estimates of the higher-band parameters. The coefficients C_0, C_1, and C_2 can thus be calculated as a function of k_F, n, or SdH frequency, whichever is desired.

*Supported in part by the U. S. Army Research Office, Durham, The Advanced Research Projects Agency, and a Faculty Research Grant from North Texas State University.

†On leave from the Institute of Physics, Polish Academy of Sciences, Warsaw, Poland.

[1]R. R. Galazka, D. G. Seiler, and W. M. Becker, J. Phys. (to be published). This was reported at the Conference on the Physics of Semimetals and Narrow Gap Semiconductors, Dallas, 1970 (unpublished).

[2]C. R. Whitsett, Phys. Rev. 138, A829 (1965).

[3]G. B. Wright, A. J. Strauss, and T. C. Harman, Phys. Rev. 125, 1534 (1962).

[4]S. S. Shalyt and S. A. Aliev, Fiz. Tverd. Tela 6, 1979 (1964) [Sov. Phys. Solid State 6, 1563 (1965)].

[5]S. A. Aliev, L. L. Korenblut, and S. S. Shalyt, Fiz. Tverd. Tela 7, 1673 (1965) [Sov. Phys. Solid State 7, 1357 (1965)].

[6]E. O. Kane, J. Phys. Chem. Solids 1, 249 (1957). See also E. O. Kane, in *Semiconductors and Semimetals*, edited by R. K. Willardson and A. C. Beer (Academic, New York, 1966), Vol. 1, p. 75.

[7]In Ref. 5 only values of E_g and m^*/m_0 were calculated.

[8]T. C. Harman, in *Physics and Chemistry of II-VI Compounds*, edited by M. Aven and J. S. Premer (North-Holland, Amsterdam, 1967), Chap. XV.

[9]L. M. Bliek and G. Landwehr, Phys. Status Solidi 31, 115 (1969).

[10]L. M. Bliek and G. Landwehr, Phys. Status Solidi 33, K67 (1969).

[11]S. H. Groves, R. N. Brown, and C. R. Pidgeon, Phys. Rev. 161, 779 (1967).

[12]D. G. Seiler and W. M. Becker, Phys. Letters 26A, 96 (1967).

[13]D. G. Seiler, W. M. Becker, and L. M. Roth, Phys. Rev. B 1, 764 (1970).

[14]S. H. Groves and P. W. Wyatt, calculations discussed in Refs. 15 and 16 (unpublished).

[15]L. M. Roth, S. H. Groves, and P. W. Wyatt, Phys. Rev. Letters 19, 576 (1967).

[16]L. M. Roth, Phys. Rev. 173, 755 (1968).

[17]D. G. Seiler and W. M. Becker, Phys. Rev. 183, 784 (1969). We take this opportunity to point out errors in Eqs. (B9), (B10), and (B11) of this paper. In each equation, a factor of 2 which multiplies the expression $(-\frac{1}{3}a)^{1/2}$ has been inadvertently omitted.

[18]J. M. Ziman, *Electrons and Phonons* (Oxford U. P., New York, 1960), p. 514.

[19]J. G. Broerman, Phys. Rev. B 2, 1818 (1970). We thank the author for communication of his work prior to

publication.
[20]P. Löwdin, J. Chem. Phys. 19, 1396 (1951).
[21]R. L. Bell and K. T. Rodgers, Phys. Rev. 152, 746 (1966).

PHYSICAL REVIEW B VOLUME 3, NUMBER 12 15 JUNE 1971

P^{31} Spin Echoes in Metallic Phosphorus-Doped Silicon*

G. P. Carver† and D. F. Holcomb
Laboratory of Atomic and Solid State Physics, Cornell University, Ithaca, New York 14850

and

J. A. Kaeck
Department of Physics, University of Illinois at Chicago Circle, Chicago, Illinois 60680
(Received 7 December 1970)

Observations of solid echoes in the P^{31} spin system in metallic Si : P are reported. Homogenous linewidths and spin-lattice relaxation times are given.

The experimental data reported herein is an extension of that reported previously by Sundfors and Holcomb.[1] It consists of spin-echo data for the P^{31} nuclear spin resonance, taken from 1.3 to 2.0 °K in two of the samples listed in Ref. 1, at phosphorus donor concentrations of 1.4×10^{20} and 9×10^{19} cm^{-3}. (These were samples P-1 and P-2 listed in Table I of Ref. 1.)

The experiments were performed using a phase-coherent pulsed NMR spectrometer designed by Clark.[2] The cryogenic system used was that described by Sundfors.[3] The experiments were conducted using a field of 50 G at 8.5 MHz. The echoes were produced by the usual 90°-τ-180° pulse sequence. T_2 was measured by changing the pulse spacing τ. T_1 was measured by observing the recovery of the echo amplitude, after the second of two such echo-producing pulse sequences, as a function of the time between sequences. The samples were immersed directly in the helium bath which was pumped below the λ point. The results of experimental tests to determine if there was Ohmic heating in the samples due to the rf pulses showed that such heating was negligible.

The experimental data for relaxation times are given in Table I, together with other relevant numbers for comparison. Figure 1 shows a spin-echo signal from sample P-2 at 1.3 °K.

The calculated value of T_2 given in the fifth column of Table I was obtained under the assumption that it is determined entirely by magnetic dipolar interaction with Si^{29} nuclear spins and with other P^{31} nuclear spins. The exponential echo-decay plots which were obtained suggest a Lorentzian shape for the homogeneous line. Consequently, we write the expression for the observed P^{31} spin-echo decay time $(T_2)_P$ as

$$1/(T_2)_P = 1/(T_2)_{P\text{-}P} + 1/(T_2)_{Si\text{-}P}\ , \qquad (1)$$

where[5]

$$1/(T_2)_{P\text{-}P} = 3.8\,\gamma_P^2\,\hbar N_D \qquad (2)$$

and[6]

$$1/(T_2)_{Si\text{-}P} \cong \gamma_P^2\,(2.5\gamma_{Si}\,\hbar N_{Si})^2/3.8\gamma_{Si}\,\hbar N_{Si}\ . \qquad (3)$$

Given the uncertainty concerning the exact applicability of Eqs. (2) and (3), the numbers in column 5 of the table, calculated on the basis of those equations, are in reasonable agreement with the experimental values of T_2 in column 4. They certainly indicate that there are no significant sources of broadening for the P^{31} resonance which are unaccounted for. (As shown in Ref. 1, there is a huge inhomogeneous broadening from the distribution in Knight shifts, giving the short value for T_2^*. The fact that the calculated values of T_2 are shorter than the experimental may, among other things, represent an effect of that Knight-shift distribution in weakening mutual spin-flip processes between

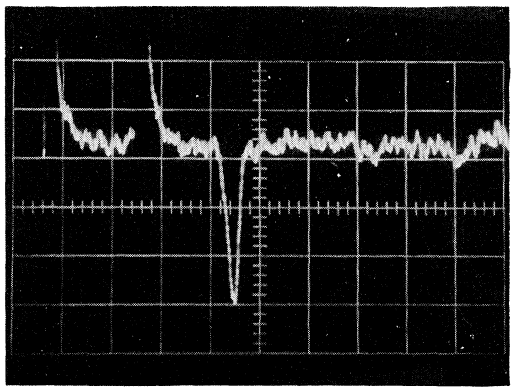

FIG. 1. Spin echo from P^{31} system at 1.3 °K, for sample with $N_D = 9\times10^{19}$ cm^{-3}. Oscilloscope is sweeping at 0.2 msec/cm.